Excited-state free energy surfaces in solution: Time-dependent density functional theory/reference interaction site model self-consistent field method

Noriyuki Minezawa

Citation: J. Chem. Phys. **138**, 244101 (2013); doi: 10.1063/1.4811201
View online: http://dx.doi.org/10.1063/1.4811201
View Table of Contents: http://jcp.aip.org/resource/1/JCPSA6/v138/i24
Published by the AIP Publishing LLC.

Excited-state free energy surfaces in solution: Time-dependent density functional theory/reference interaction site model self-consistent field method

Noriyuki Minezawa[a)]
Fukui Institute for Fundamental Chemistry, Kyoto University, Sakyo-ku, Kyoto 606-8103, Japan

(Received 4 April 2013; accepted 31 May 2013; published online 25 June 2013)

Constructing free energy surfaces for electronically excited states is a first step toward the understanding of photochemical processes in solution. For that purpose, the analytic free energy gradient is derived and implemented for the linear-response time-dependent density functional theory combined with the reference interaction site model self-consistent field method. The proposed method is applied to study (1) the fluorescence spectra of aqueous acetone and (2) the excited-state intramolecular proton transfer reaction of *ortho*-hydroxybenzaldehyde in an acetonitrile solution. © *2013 AIP Publishing LLC*. [http://dx.doi.org/10.1063/1.4811201]

I. INTRODUCTION

Solvent effects play a vital role in photochemistry of molecules in solution. Experiments have made tremendous progress in understanding solvent effects by using both steady-state absorption and fluorescence spectra and time-resolved techniques. Solvatochromic shifts, for example, reflect the strength of solute-solvent interaction that depends critically on the solute electronic structure.[1] Since polar solvents stabilize ionic states more effectively than covalent states, not only the energy gap but also the order of electronic states changes upon solvation. It is not surprising that the presence of polar solvent alters significantly the excited-state lifetime and even relaxation mechanism. Therefore, the identification of stationary points and reaction paths in solution provides valuable insight into the mechanisms of relaxation processes. Constructing equilibrium free energy surfaces is a convenient approach to examine photochemistry in solution, although the relevant processes generally occur in non-equilibrium regime.

Reference interaction site model self-consistent field (RISM-SCF) method[2–11] has been successfully applied to free energy calculations for molecules in solution. The RISM-SCF is the hybrid approach of *ab initio* electronic structure methods for solute and RISM integral equation theory for solvent. The solute electron density and solvation structure are determined in a self-consistent fashion. In addition, the RISM-SCF can locate minimum free energy points with reasonable computational costs, because the method does not require extensive sampling like conventional quantum mechanics/molecular mechanics (QM/MM) molecular dynamics simulation. The RISM approach has been combined with various electronic structure methods including Hartree-Fock,[2] complete active space SCF (CASSCF),[3] single-reference second-order Møller-Plesset perturbation theory (MP2),[7] and multi-state second-order perturbation theory with CASSCF reference (MS-CASPT2).[8]

The linear-response time-dependent density functional theory (LR-TDDFT)[12–20] is an efficient method of computing the electronically excited states. Incorporating environmental effects, the method has been successfully applied to predict absorption and emission spectra of complex molecular systems.[21,22] Recently, several hybrid methods of LR-TDDFT and solvent models have been developed using both implicit and explicit solvents. In the former, the polarizable continuum model (PCM) is one of the useful approaches that incorporate solvent effects very efficiently, and has been widely employed to compute spectra of molecules in solution.[21–27] In the latter category, *ab initio*-based polarizable solvent models have been combined with the LR-TDDFT,[28–30] and a three-layer LR-TDDFT/explicit solvent/implicit solvent approach is also available.[31]

In the present work, the RISM-SCF method is combined with the LR-TDDFT. Kaminski *et al.*[32] have examined the solvatochromic shift using the embedding potential within the LR-TDDFT method. These authors construct the statistically averaged electron density of solvent by using the solvent site distributions derived from the three-dimensional RISM theory. Recently, Fernandez and Sato[33] have reported the LR-TDDFT absorption spectra of the nitroxy radical in several solvents on the basis of the RISM-DFT ground-state solvation structure. In contrast to the simulation of absorption spectra, the computation of fluorescence spectra is challenging because the steady-state emission originates from the excited-state minimum geometry. Therefore, it is important to develop the analytic free energy gradient for the RISM-TDDFT method. The main purpose of the present study is the implementation of the analytic free energy gradient in order to explore the excited-state free energy surfaces in solution.

The organization of this paper is as follows. In Sec. II, the analytic free energy gradient for the RISM-TDDFT method is derived. Section III presents the calculated results of (1) the fluorescence spectra of aqueous acetone and (2) the free energy surfaces for the excited-state intramolecular proton transfer (ESIPT) reaction of *ortho*-hydroxybenzaldehyde

[a)]E-mail: minezawa@fukui.kyoto-u.ac.jp

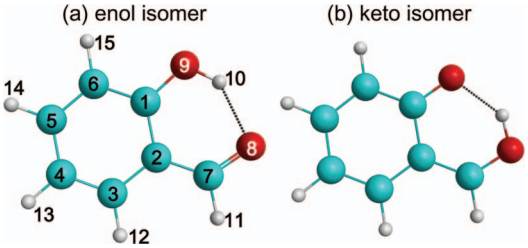

FIG. 1. (a) enol and (b) keto isomers of *ortho*-hydroxybenzaldehyde (OHBA): carbon (cyan), oxygen (red), and hydrogen (white) atoms.

(OHBA) illustrated in Fig. 1. Section IV concludes the present work.

II. THEORETICAL APPROACH

A. TDDFT/RISM method

The Helmholtz free energy at the RISM-DFT level is defined as the sum of solute electronic energy functional $E_{\rm solute}$ and excess chemical potential $\Delta\mu$,

$$\mathcal{G}_{\rm ref}[n] = E_{\rm solute}[n] + \Delta\mu[n], \tag{1}$$

where $E_{\rm solute}[n]$ is the usual Kohn-Sham (KS) energy functional.[34] The second term $\Delta\mu[n]$, which is evaluated using the solute-solvent correlation functions taken from the RISM equations, also has functional dependence on the solute electron density $n(\mathbf{r})$. On the basis of the variational formulation developed in Refs. 2 and 3, the so-called solvated Fock matrix is derived as follows:

$$F^{\rm solv}_{pq\sigma}(\mathbf{r}) = F^{\rm gas}_{pq\sigma}(\mathbf{r}) + v^{\rm RISM}_{pq\sigma}(\mathbf{r}). \tag{2}$$

Here, $F^{\rm gas}_{pq\sigma}(\mathbf{r})$ is the usual KS Fock matrix, and $v^{\rm RISM}_{pq\sigma}(\mathbf{r})$ is the RISM potential:

$$v^{\rm RISM}_{pq\sigma}(\mathbf{r}) \equiv \int d\mathbf{r}\psi_{p\sigma}(\mathbf{r})\frac{\delta\Delta\mu}{\delta n_\sigma(\mathbf{r})}\psi_{q\sigma}(\mathbf{r}) = \sum_\alpha^{\rm sites}(\hat{Q}^\alpha)_{pq\sigma}V^\alpha. \tag{3}$$

Hereafter, indices $i, j, \ldots$ label occupied, $a, b, \ldots$ virtual, and $p, q, \ldots$ general molecular orbitals (MO), and Greek letters σ and τ are spin labels. The superscript $\alpha, \beta, \gamma, \ldots$ denotes the solute site. $\hat{Q}^\alpha$ and V^α are the charge generation operator and the electrostatic potential (ESP) acting on the solute site, respectively. Note that the ESP V^α depends on the solute electron density because the ESP is constructed from the site-site radial distribution functions that reflect the solute potential in solving the RISM equations.

The excited-state free energy for the RISM-TDDFT is defined as

$$\mathcal{G} = \mathcal{G}_{\rm ref} + \Omega. \tag{4}$$

The excitation energy Ω is a solution of the non-Hermitian matrix equation,

$$\begin{pmatrix}\mathbf{A} & \mathbf{B}\\ \mathbf{B} & \mathbf{A}\end{pmatrix}\begin{pmatrix}\mathbf{X}\\ \mathbf{Y}\end{pmatrix} = \Omega\begin{pmatrix}\mathbf{1} & \mathbf{0}\\ \mathbf{0} & -\mathbf{1}\end{pmatrix}\begin{pmatrix}\mathbf{X}\\ \mathbf{Y}\end{pmatrix}, \tag{5}$$

where

$$A_{ia\sigma,jb\tau} = (\varepsilon_{a\sigma} - \varepsilon_{i\sigma})\delta_{ij}\delta_{ab}\delta_{\sigma\tau} + K_{ia\sigma,jb\tau}, \tag{6}$$

$$B_{ia\sigma,jb\tau} = K_{ia\sigma,bj\tau}. \tag{7}$$

Here δ_{pq} is the Kronecker delta, and $\mathbf{X}$ and $\mathbf{Y}$ denote the transition amplitudes. The ground-state RISM-SCF affects Eqs. (5)–(7). First, the MO coefficients and orbital energies $\varepsilon_{p\sigma}$ are obtained by solving the ground-state KS equation with the solvated Fock operator defined in Eq. (2). Second, the coupling matrix K is modified because the RISM potential is dependent on the electron density,

$$K_{ia\sigma,jb\tau} = K^{\rm gas}_{ia\sigma,jb\tau} + f^{\rm RISM}_{ia\sigma,jb\tau}, \tag{8}$$

where

$$f^{\rm RISM}_{ia\sigma,jb\tau} = \int\int d\mathbf{r}d\mathbf{r}'\psi_{i\sigma}(\mathbf{r})\psi_{a\sigma}(\mathbf{r})\frac{\delta v^{\rm RISM}_\sigma(\mathbf{r})}{\delta n_\tau(\mathbf{r}')}\psi_{j\tau}(\mathbf{r}')\psi_{b\tau}(\mathbf{r}') = \sum_{\alpha\beta}^{\rm sites}(\hat{Q}^\alpha)_{ia\sigma}\frac{\partial V^\alpha}{\partial Q^\beta}(\hat{Q}^\beta)_{jb\tau}. \tag{9}$$

The ESP derivative $\partial\mathbf{V}/\partial\mathbf{Q}$ is evaluated solving the first-order coupled-perturbed RISM (CP-RISM) equations.[5]

In the present RISM-TDDFT approach, the excitation energy Ω in Eq. (4) is *not* identical with the vertical transition energy in solution because of the RISM kernel $f^{\rm RISM}$ contribution:

$$\sum_{ia\sigma,jb\tau} X_{ia\sigma}f^{\rm RISM}_{ia\sigma,jb\tau}X_{jb\tau} = \sum_\alpha^{\rm sites}{\rm Tr}(\hat{Q}^\alpha\mathbf{X})\sum_\beta^{\rm sites}\frac{\partial V^\alpha}{\partial Q^\beta}{\rm Tr}(\hat{Q}^\beta\mathbf{X}). \tag{10}$$

For brevity, $\mathbf{Y} = \mathbf{0}$ is assumed here. Equation (10) accounts for the coupling between the electronic excitation and the ESP within the linear-response regime. This term indicates the interaction energy between the transition-density charges and the ESP change due to the transition density. In the RISM theory, however, the ESP constitutes a slow component of solvation and cannot respond to solute electronic excitation quickly. Thus, the contribution of Eq. (10) is set to be zero in the computation of vertical transition energies; the ESP is thought of as an external potential. In contrast, the RISM kernel plays an important role in calculating excited-state free energies [Eq. (4)], because this term partially accounts for the solvent relaxation expected in electronically excited states.

The analytic gradient of Eq. (4) is easily derived by modifying the gas-phase TDDFT analytic energy gradient:[20] the exchange-correlation kernel $f^{\rm xc}$ is simply read as $f^{\rm xc} + f^{\rm RISM}$. In the gradient computation, the third functional derivatives are involved, and the corresponding RISM term is

$$g^{\rm RISM}(\mathbf{r},\mathbf{r}',\mathbf{r}'') = \sum_{\alpha\beta\gamma}^{\rm sites}\frac{\partial^2 V^\alpha}{\partial Q^\beta\partial Q^\gamma}\hat{Q}^\alpha(\mathbf{r})\,\hat{Q}^\beta(\mathbf{r}')\hat{Q}^\gamma(\mathbf{r}''), \tag{11}$$

where the second derivative of ESP is calculated by the second-order CP-RISM equation.[6,7]

The RISM affects the TDDFT gradient through the potential v^{RISM} and kernel f^{RISM}. In the atomic basis set expression (μ, ν, κ, λ indexes atomic basis function), the gradient with respect to nuclear coordinate ξ is given by

$$\Omega^{\mathrm{RISM},\xi} = \sum_{\mu\nu\sigma} v^{\mathrm{RISM},(\xi)}_{\mu\nu\sigma} P_{\mu\nu\sigma} + \sum_{\mu\nu\sigma,\kappa\lambda\tau} f^{\mathrm{RISM},(\xi)}_{\mu\nu\sigma,\kappa\lambda\tau} (\mathbf{X}+\mathbf{Y})_{\mu\nu\sigma} (\mathbf{X}+\mathbf{Y})_{\kappa\lambda\tau}, \quad (12)$$

where $\mathbf{P}$ is the relaxed difference density matrix obtained by solving the CP-KS equation. The parenthesized symbol (ξ) denotes that the derivative with respect to ξ is taken with keeping the MO coefficients frozen at the RISM-DFT values. The first term of Eq. (12) is

$$\begin{aligned}
&\sum_{\mu\nu\sigma} P_{\mu\nu\sigma} \left[\sum_{\alpha}^{\text{sites}} (\hat{Q}^{\alpha})_{\mu\nu\sigma} V^{\alpha} \right]^{(\xi)} \\
&= \sum_{\mu\nu\sigma} P_{\mu\nu\sigma} \sum_{\alpha}^{\text{sites}} (\hat{Q}^{\alpha})_{\mu\nu\sigma} \left[\left(\frac{\partial V^{\alpha}}{\partial \xi} \right)_{\mathbf{Q}} + \sum_{\beta}^{\text{sites}} \left(\frac{\partial V^{\alpha}}{\partial Q^{\beta}} \right) (Q^{\beta})^{(\xi)} \right] \\
&\quad + \sum_{\mu\nu\sigma} P_{\mu\nu\sigma} \sum_{\alpha}^{\text{sites}} (\hat{Q}^{\alpha})^{(\xi)}_{\mu\nu\sigma} V^{\alpha} \\
&= \sum_{\alpha}^{\text{sites}} \left[(Q^{\alpha})^{\Delta} \left(\frac{\partial V^{\alpha}}{\partial \xi} \right)_{\mathbf{Q}} + V^{\alpha} (Q^{\alpha})^{\Delta,(\xi)} \right] \\
&\quad + \sum_{\alpha\beta}^{\text{sites}} (Q^{\alpha})^{\Delta} \frac{\partial V^{\alpha}}{\partial Q^{\beta}} (Q^{\beta})^{(\xi)}. \qquad (13)
\end{aligned}$$

Here, $\mathbf{Q} = \mathrm{Tr}(\mathbf{D}\hat{\mathbf{Q}})$ and $\mathbf{Q}^{\Delta} = \mathrm{Tr}(\mathbf{P}\hat{\mathbf{Q}})$ are site charges generated by the ground-state KS density matrix $\mathbf{D}$ and the relaxed difference density matrix $\mathbf{P}$, respectively. The subscript $\mathbf{Q}$ in the first term of Eq. (13) indicates that the derivative is taken with keeping $\mathbf{Q}$ constant.

The second term of Eq. (12) is given by

$$\begin{aligned}
&\sum_{\mu\nu\sigma,\kappa\lambda\tau} f^{\mathrm{RISM},(\xi)}_{\mu\nu\sigma,\kappa\lambda\tau} (\mathbf{X}+\mathbf{Y})_{\mu\nu\sigma} (\mathbf{X}+\mathbf{Y})_{\kappa\lambda\tau} \\
&= \sum_{\mu\nu\sigma,\kappa\lambda\tau} \sum_{\alpha\beta}^{\text{sites}} \left[(\hat{Q}^{\alpha})_{\mu\nu\sigma} \frac{\partial V^{\alpha}}{\partial Q^{\beta}} (\hat{Q}^{\beta})_{\kappa\lambda\tau} \right]^{(\xi)} \\
&\quad \times (\mathbf{X}+\mathbf{Y})_{\mu\nu\sigma} (\mathbf{X}+\mathbf{Y})_{\kappa\lambda\tau} \\
&= \sum_{\alpha\beta}^{\text{sites}} (Q^{\alpha})^{X+Y} \left[\frac{\partial}{\partial \xi} \left(\frac{\partial V^{\alpha}}{\partial Q^{\beta}} \right) \right]_{\mathbf{Q}} (Q^{\beta})^{X+Y} \\
&\quad + \sum_{\alpha\beta\gamma}^{\text{sites}} \frac{\partial^2 V^{\alpha}}{\partial Q^{\beta} \partial Q^{\gamma}} (Q^{\alpha})^{X+Y} (Q^{\beta})^{X+Y} (Q^{\gamma})^{(\xi)} \\
&\quad + 2 \sum_{\alpha\beta}^{\text{sites}} (Q^{\alpha})^{X+Y} \frac{\partial V^{\alpha}}{\partial Q^{\beta}} (Q^{\beta})^{X+Y,(\xi)}, \qquad (14)
\end{aligned}$$

where $\mathbf{Q}^{X+Y} = \mathrm{Tr}[(\mathbf{X}+\mathbf{Y})\hat{\mathbf{Q}}]$. The ESP derivatives with respect to the site charges and nuclear coordinates are evaluated by solving the first- and second-order CP-RISM equations.[5–7]

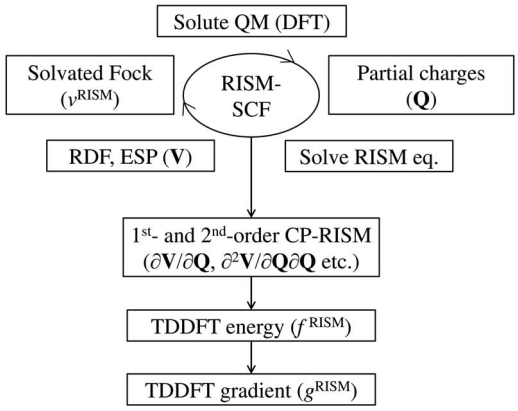

FIG. 2. Scheme of the RISM-TDDFT computation.

The RISM-TDDFT scheme is summarized in Fig. 2. First, the ground-state RISM-DFT calculation is performed. The solute electron density and solvation structure (ESP) are determined to be self-consistent. After the RISM-DFT is converged, the first- and second-order CP-RISM equations are solved to obtain the ESP derivative terms. Then the LR-TDDFT energy and gradient computation is performed using these variables. It should be noted that in the LR regime the RISM-SCF convergence is achieved at the ground-state DFT level. Therefore, the increase of computational cost is marginal for the TDDFT step.

B. Corrections for LR approach

The LR approach adopted in this work has difficulty in realizing a true equilibrium solvation for excited state. The RISM equations are solved under the ground-state solute, and the solvation structure has no dependence on the excited-state density. The self-consistency is not taken into account for the excitation energy calculations, although some first-order interaction terms appear in the gradient formulation. Such self-consistency is beyond the LR approximation, and state-specific calculations are desirable to obtain fully self-consistent solute-solvent equilibrium structures. A state-specific version of PCM (SS-TDDFT-PCM), for example, has been developed and the results are compared with those by LR-TDDFT-PCM method.[24–26] Recently, Sneskov *et al.*[35] have discussed the mutual electronic polarization for the LR-based QM method.

One needs excited-state equilibrium solvation structures to compute fluorescence spectra. In this work, the emission energies are computed using the excited-state ESP obtained by Taylor expansion around the ground-state ESP:

$$\begin{aligned}
&\text{ESP-0}: \quad V^{\alpha}(\mathrm{S}_0), \\
&\text{ESP-1}: \quad V^{\alpha}(\mathrm{S}_0) + \sum_{\beta}^{\text{sites}} \frac{\partial V^{\alpha}}{\partial Q^{\beta}} \Delta Q^{\beta}, \\
&\text{ESP-2}: \\
&\quad V^{\alpha}(\mathrm{S}_0) + \sum_{\beta}^{\text{sites}} \frac{\partial V^{\alpha}}{\partial Q^{\beta}} \Delta Q^{\beta} + \frac{1}{2} \sum_{\beta\gamma}^{\text{sites}} \frac{\partial^2 V^{\alpha}}{\partial Q^{\beta} \partial Q^{\gamma}} \Delta Q^{\beta} \Delta Q^{\gamma}, \qquad (15)
\end{aligned}$$

where $\Delta\mathbf{Q}$ is the charge difference between the ground and excited states. Here, $\mathbf{V}(S_0)$, $\partial\mathbf{V}/\partial\mathbf{Q}$, and $\partial^2\mathbf{V}/\partial\mathbf{Q}\partial\mathbf{Q}$ are obtained by the ground-state RISM-DFT. The "ESP-*N*" denotes the *N*th order expansion of ESP. Note that ESP-0 is identical to the ground-state ESP. The excited-state free energy is modified according to the corrected LR approach in Refs. 25 and 30. The resultant correction term is given by

$$\frac{1}{2}\sum_{\alpha\beta}^{\text{sites}}\frac{\partial V^{\alpha}}{\partial Q^{\beta}}\Delta Q^{\alpha}\Delta Q^{\beta}. \tag{16}$$

In the present RISM-TDDFT case, $\Delta\mathbf{Q}$ in Eqs. (15) and (16) is set equal to be $\mathbf{Q}^{\Delta}$ generated by the relaxed difference electron density.

C. Computational details

The RISM-TDDFT method is applied to (1) the fluorescence spectra of aqueous acetone and (2) the ESIPT reaction of OHBA in an acetonitrile solution. The RISM code was interfaced with the program package GAMESS.[36,37] The solute electronic structure was described at the (TD-)DFT level; B3LYP functional[38,39] and cc-pVDZ basis set[40] were employed. The site-site RISM equations were solved with the hyper-netted-chain closure. In all calculations, the temperature was fixed at 298.15 K. The solute Lennard-Jones (LJ) parameters were taken from the AMBER force field.[41] The standard combination rule was applied to evaluate the solute-solvent LJ interaction potential.

For aqueous acetone, the simple point charge (SPC) model[42] was adopted for water. The density of solvent was set to be 1.0 g/cm^3. For the ESIPT reaction of OHBA, three-site model by Jorgensen and Briggs[43] was used for the acetonitrile solvent. The density was set to be 0.777 g/cm^3. The LJ parameter $\sigma = 1.0$ Å and $\varepsilon = 0.056$ kcal/mol was assigned to the transferred proton. The reaction coordinate was chosen as the difference between two OH bond lengths (see Fig. 1):

$$s = \frac{1}{2}\left[r(O_9H_{10}) - r(O_8H_{10})\right],$$

where O_9 and O_8 are the donor and acceptor oxygen atoms, and minus (plus) s corresponds to the enol (keto) tautomer. Since the enol form is dominant in the ground-state, the ESIPT proceeds from enol to keto, and s changes from negative to positive values. For a given value of s, the geometry was determined by optimizing the remaining degrees of freedom. The C_s symmetry was imposed to obtain the $n\pi^*$ ($1A''$) and $\pi\pi^*$ ($2A'$) excited states, and the geometry optimization was performed for each electronic state to obtain the potential (free) energy curves.

III. RESULTS AND DISCUSSION

A. Acetone in water

The first example is the aqueous acetone system, which has been intensively examined both experimentally and theoretically.[29,44–52] The hybrid method of QM and solvent models has been applied to simulate the absorption and emission spectra.[29,45] The present application concentrates on the minimum free energy geometry of $n\pi^*$ state and the relevant emission energy. Table I summarizes the optimized geometries for the ground and $n\pi^*$ states. For the ground state, the C=O bond length is stretched by 0.01 Å while the C–C bonds shrink by 0.01 Å in transferring from vacuum to solution. The dipole moment increases by 1.3 D. In the $n\pi^*$ state, the C=O group is pyramidalized due to the electron migration from n to π^* orbital. The enhancement of wagging mode is observed in solution; the out-of-plane angle (∠O–CCC) increases by 4°. The solvent-induced change in the dipole is moderate for the $n\pi^*$ state compared to the ground state.

TABLE I. Selected geometric parameters of acetone optimized at the (TD-)B3LYP/cc-pVDZ level. Bond lengths are given in angstroms (Å), angles in degrees (°), and dipole moments in Debye (D).[a]

	Gas		Water	
	S_0	$n\pi^*$	S_0	$n\pi^*$
r(CO)	1.214 (1.220)	1.316 (1.355)	1.225	1.309
r(CC)	1.520 (1.520)	1.508 (1.521)	1.507	1.521
∠CCC	116.4 (116.2)	120.2 (117.3)	117.2	117.8
∠O–CCC	0.0 (0.0)	32.3	0.0	36.5
Dipole	2.71	1.85	4.08	2.32

[a]CASSCF(11,10)/6-311G(d,p) values in Ref. 44 are included in parentheses.

Table II shows the vertical transition energies of acetone in gas and aqueous solution phases. The ground-state optimal ESP is employed to compute the absorption energy in water. The TD-B3LYP/cc-pVDZ excitation energies are calculated to be 4.40 and 4.61 eV in gas and water, respectively. These values are comparable to those by previous studies.[29,44,45] The solvatochromic shift is estimated to be 0.21 eV, which is also in close agreement with the experiments.

In the RISM-TDDFT emission energy calculations, the approximate ESP in Eq. (15) is employed to mimic the excited-state equilibrium solvation structure. Before computing the fluorescence spectra, the accuracy of present extrapolation scheme is examined. For that purpose, the RISM-CASSCF method is adopted because the method can determine a state-specific equilibrium solvation structure for both the ground and $n\pi^*$ states. The active space consists of five orbitals (π, σ, n, π^*, σ^*), and six electrons are distributed among them, i.e., CASSCF(6,5). The RISM-CASSCF calculations are performed at the RISM-TDDFT optimized geometry, and the ESP and its derivative terms are obtained. At the RISM-CASSCF level, the maximum (root-mean-square) difference between the state-specific ($n\pi^*$) and approximate ESP is estimated to be 0.06 (0.03), 0.30 (0.12), and 0.93 (0.40) V for ESP-2, ESP-1, and ESP-0, respectively. A remarkable improvement is achieved even at ESP-1, and a nearly perfect agreement is observed for ESP-2. On the contrary, the ground-state ESP (ESP-0) differs considerably from the $n\pi^*$ counterpart; the maximum difference of 0.93 eV, for instance, indicates a large discrepancy of solvation structure around the carbonyl oxygen atom. Therefore, the ESP-2 scheme is shown to be a good approximation for the excited-state ESP.

The RISM-TDDFT emission energies are computed to be 2.96, 2.92, and 3.30 eV by using ESP-2, ESP-1, and ESP-0, respectively. The ESP-2 and ESP-1 predict redshift (−0.07 and −0.11 eV), while the ESP-0 predicts blueshift

TABLE II. Vertical transition energies (eV) of acetone in vacuum and aqueous solution.

	Absorption ($n \rightarrow \pi^*$)		Emission ($\pi^* \rightarrow n$)	
	Gas	Water	Gas	Water
RISM/TD-B3LYP/cc-pVDZ	4.40	4.61	3.03	2.96/2.92/3.30[a]
RISM/MRMP/cc-pVDZ[b]	4.43	4.66		
EFP/TD-B3LYP/DZP[c]	4.38	4.59		
ROKS-MD[d]	3.85 ± 0.09	4.10 ± 0.11	2.46 ± 0.11	2.45 ± 0.26
Expt.	4.48[e], 4.49[f]	4.68[f], 4.69[e,i]	~3.0[g]	~3.1[h]

[a]ESP-2/ESP-1/ESP-0, see Eq. (15).
[b]RISM-CASSCF(6,5) geometry optimization followed by a single-point multi-reference Møller-Plesset perturbation theory (MRMP) calculation.
[c]Average excitation energies taken from the ground-state B3LYP and B3LYP/effective fragment potential MD snapshots, Ref. 29.
[d]Average excitation energies taken from restricted-open KS MD using BLYP functional and TIP3P water, Ref. 45.
[e]Reference 49.
[f]Reference 46.
[g]In *n*-hexane, Refs. 50 and 52.
[h]Reference 51.
[i]References 47 and 48.

(+0.27 eV). Both ESP-2 and ESP-1 values are in good agreement with those of other theoretical methods, although experiments predict a slight blueshift. Again, the ESP-0 performance is poor. The ESP-0 is the ground-state ESP which is invalid for the emission energy calculations, and the large blueshift implies the overstabilization of the ground state. A qualitative difference in solvatochromic shift indicates a crucial role of ESP correction. In the LR regime, the proposed scheme [Eq. (15)] can provide more appropriate ESP that mimics the equilibrium solvation structures for excited states.

B. ESIPT of OHBA in acetonitrile

The second example is the ESIPT reaction of OHBA (see Fig. 1) in acetonitrile solvent. The ESIPT is one of the fundamental processes in photochemistry and photobiology,[53,54] and the reaction dynamics is examined extensively by experiments using femtosecond spectroscopies.[55] Since the molecule is sufficiently small, a large number of studies have been performed to understand the mechanism of ESIPT.[56–73] For the OHBA, marginal solvent effects are observed in experiments. Catalán *et al.*[57] have reported very similar absorption (emission) maxima: 327 (525) nm in cyclohexane and 325 (525 ± 5) nm in aprotic polar *N*,*N*-dimethylformamide. Furthermore, polar solvents accelerate only very slightly fluorescence decay: 2.3×10^{10} s^{-1} and 1.9×10^{10} s^{-1} in acetonitrile and nonpolar 3-methylpentane, respectively.[59] Although polar solvents play a minor role in the ESIPT dynamics of OHBA, recent experimental studies have shown drastic changes in reaction rate of ESIPT for other photo acid.[74] Therefore, the present application is a first step to examine ESIPT reactions for these molecular systems that receive considerable attention.

The ESIPT reaction of OHBA proceeds without any barrier. The time-resolved photoelectron spectroscopy[65] supports this view. The previous theoretical studies[67–70] have shown that the ESIPT proceeds without any barrier for the $\pi\pi^*$ state while there exists a sizable barrier along the PT coordinate for the $n\pi^*$ state. In the *ab initio* multiple spawning simulation study, Coe and Martinez[71] found the keto- and enol-like conical intersections between the $n\pi^*$ and $\pi\pi^*$ states and investigated the role of dark $n\pi^*$ state that is involved in the ESIPT and internal conversion processes. Migani *et al.*[72] determined the extended conical intersection seam and discussed the decay paths on the basis of the seam structure. Since the $n\pi^*$ and $\pi\pi^*$ states are nearly degenerate at the Franck-Condon region, it is interesting to see how polar solvents affect the free energy profiles along the PT coordinate.

Table III summarizes the optimized geometric parameters. Four important geometries are shown: S_0 (enol), $n\pi^*$ (keto and enol), and $\pi\pi^*$ (keto). Note that the solution-phase $n\pi^*$ geometries are not true minimum due to the C_s symmetry

TABLE III. Selected geometric parameters of OHBA optimized at the RISM-(TD-)B3LYP/cc-pVDZ level. Bond lengths are given in angstroms (Å), angles in degrees (°), and dipole moments in Debye (D).[a] Atom numbering is given in Fig. 1.

	S_0 (enol)	$n\pi^*$ (enol)[b]	$n\pi^*$ (keto)[b]	$\pi\pi^*$ (keto)
$r(O_9H_{10})$	0.995 (0.995)	0.978 (0.976)	1.772 (1.740)	1.530 (1.477)
$r(O_8H_{10})$	1.710 (1.708)	1.830 (1.815)	0.982 (0.982)	1.043 (1.064)
$r(O_8O_9)$	2.607 (2.610)	2.657 (2.655)	2.580 (2.565)	2.509 (2.486)
$r(C_7O_8)$	1.236 (1.234)	1.308 (1.309)	1.341 (1.340)	1.319 (1.311)
$\angle C_6O_9H_{10}$	106.8 (106.4)	111.9 (111.1)	107.7 (107.7)	101.5 (101.2)
$\angle C_7O_8H_{10}$	99.8 (99.4)	99.4 (98.4)	111.0 (109.7)	103.9 (103.2)
$\angle O_8H_{10}O_9$	148.1 (148.7)	140.4 (142.2)	137.2 (139.1)	153.9 (155.7)
Dipole	3.29 (2.74)	2.22 (1.68)	1.13 (1.03)	5.03 (4.23)

[a]Gas-phase values are included in parentheses.
[b]Due to the C_s symmetry constraint, the solution-phase optimized geometries for $n\pi^*$ state are not true minimum.

TABLE IV. Vertical transition energies (eV) of OHBA in gas and acetonitrile solvent obtained by (TD-)B3LYP/cc-pVDZ.[a]

	Gas	Acetonitrile
Absorption		
S_0 (enol) → $n\pi^*$	3.94	3.97
S_0 (enol) → $\pi\pi^*$	3.90 (3.8-3.9[a])	3.91
Fluorescence		
$n\pi^*$ (enol) → S_0	3.37	3.31/3.31/3.46[b]
$n\pi^*$ (keto) → S_0	2.61	2.62/2.62/2.74[b]
$\pi\pi^*$ (keto) → S_0	2.69 (2.4-2.5[a])	2.66/2.66/2.74[b]

[a]Experiments conducted in vacuum (Refs. 57 and 61), 3-methylpentane (Ref. 59), and argon matrix (Ref. 63).
[b]ESP-2/ESP-1/ESP-0, see Eq. (15).

constraint. Each structure has one imaginary frequency corresponding to the out-of-plane (a'') mode. The largest amplitude is due to the transferred proton (formyl hydrogen) for the enol (keto) isomer, respectively. A polar acetonitrile solvent has a marginal influence on the ground-state geometry, while a slight change in geometric parameters is observed only for the keto isomer. The bond distances $r(O_9H_{10})$ and $r(O_8O_9)$ increase by 0.03-0.05 and 0.02 Å, respectively, implying that the intermolecular solute-solvent interaction around the O_9 atom weakens the intramolecular hydrogen bond network. In addition, the solvent pulls the transferred proton out of solute OHBA; the angle $\angle O_9H_{10}O_8$ decreases by ∼2°. The solvent-induced solute electronic polarization is weak, and the dipole moment is increased by less than 1 D for all four structures.

Table IV shows the vertical transition energies of OHBA in gas and acetonitrile solvent. The present calculations reproduce the experimental values as well as previous theoretical results by the LR-TDDFT and CASPT2. The absorption energy is calculated to be 3.90 and 3.91 eV in the gas and solution phases, and these values are comparable to those by experiments conducted in vacuum,[57,61] 3-methylpentane solvent,[59] and argon matrix.[63] The emission energies are computed to be 3.31, 2.62, and 2.66 eV for $n\pi^*$ (enol), $n\pi^*$ (keto), and $\pi\pi^*$ (keto), respectively. Very small solvatochromic shifts are obtained for both absorption and emission spectra. This is true for the Stokes shift, i.e., the difference between the absorption and emission energies. Although the Stokes shifts themselves are very large in the gas phase, indicating large geometric relaxation occurs in the excited states, the solvent-induced shifts are very small. Thus, the geometric relaxation is dominant over the solvent reorganization in the excited states.

Figure 3(a) shows the potential and free energy curves along the PT coordinate. For the $n\pi^*$ state, there exists a large barrier between the enol and keto isomers. The dipole moment of enol is larger than that of keto (2.22 and 1.13 D in solution), and the larger stabilization of the reactant enol gives rise to the increase in barrier height: 4.0 kcal/mol compared to 3.1 kcal/mol in the gas phase. At the same time, the energy difference between keto and enol isomers is reduced to be 2.8 kcal/mol.

It is the solvent relaxation that accounts for the free energy shift of ∼0.1 eV observed for the $\pi\pi^*$ state. At the ground-state minimum, the $\pi\pi^*$ vertical free energy, the second term of Eq. (4), is calculated to be 3.84 eV, while the vertical excitation energy is 3.91 eV. The resultant energy difference is attributed to the solvent relaxation in the excited state due to the RISM kernel contribution [see Eq. (10)]. The similar energy difference is also observed for the $\pi\pi^*$ keto minimum; the vertical free energy and the emission energy with the ESP-0 are 2.65 and 2.74 eV, respectively.

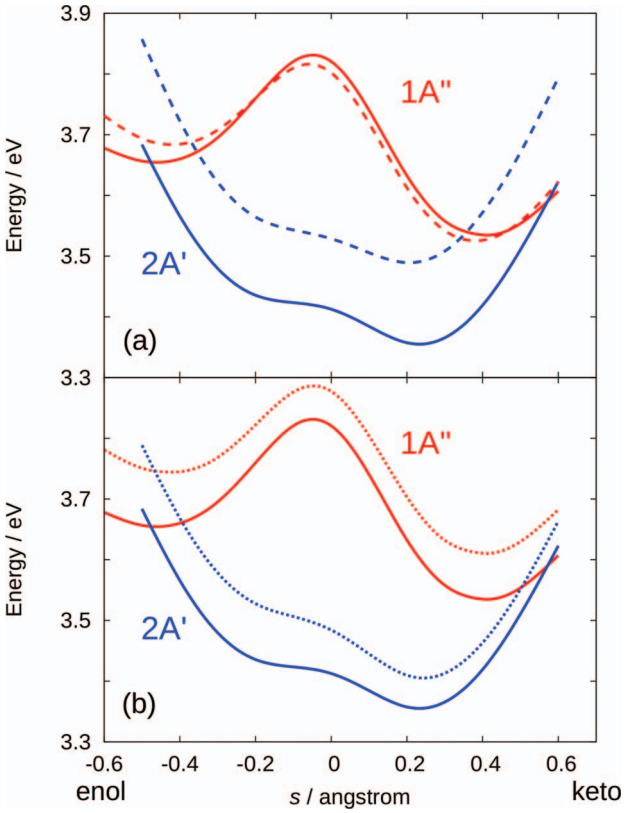

FIG. 3. (a) Solution-phase free energy (solid) and gas-phase potential energy (dashed) curves along the proton-transfer reaction coordinate: $n\pi^*$ (red) and $\pi\pi^*$ (blue) states. (b) RISM-TD-B3LYP/cc-pVDZ free energy profiles: corrected (solid) and uncorrected (dotted).

In contrast to the free energy shift, the solvent-induced spectral shift is negligible for the $\pi\pi^*$ state. This is because the ESP that is optimal for the initial state stabilizes the final state to some extent. To clarify this point, the vertical transition energies are computed by turning off the ESP. At the ground-state minimum, the solute electronic energy under the influence of ESP is decreased by 0.24 and 0.23 eV for the ground and $\pi\pi^*$ states. At the $\pi\pi^*$ keto minimum, the solute electronic energy using the ESP-2 is decreased by 0.32 and 0.35 eV for the ground and $\pi\pi^*$ states. The solute-solvent interaction stabilizes the final state more or less, and this is the reason why the solvent-induced shift is negligible.

As in the previous studies,[67–70] the present calculations predict that the $\pi\pi^*$-state ESIPT reaction proceeds without any barrier even in vacuum. In contrast to the $n\pi^*$ state, polar acetonitrile solvent stabilizes the $\pi\pi^*$ state uniformly, and the $\pi\pi^*$ state is below the $n\pi^*$ state for the almost entire range of the PT coordinate. The gas- and solution-phase energy curves are nearly parallel to each other. It is likely that the ESIPT reaction proceeds in a similar rate once the molecule reaches the

$\pi\pi^*$ state. The constant shift supports the experimental observation of small solvent effects on the fluorescence decay rate.

Finally, the free energy correction proposed in Eq. (16) is examined. Figure 3(b) shows the free energy curves with and without correction. Although the contribution of correction term is appreciable (~0.1 eV) at every point, an almost constant shift is observed for both electronic states. The free energy correction scheme proposed in this work is a convenient way of taking account of excited-state equilibrium solvation structures. Further comparative studies are needed to justify this point.

IV. CONCLUDING REMARKS

In this work, the excited-state free energy surfaces are constructed using the RISM-TDDFT method within the LR regime. The analytic free energy gradient is derived and implemented. The proposed method is applied to study (1) the fluorescence spectra of aqueous acetone and (2) the ESIPT reaction of OHBA in acetonitrile solvent. For aqueous acetone, the calculated emission energy is in close agreement with experimental values when one employs the appropriate excited-state ESP obtained by the extrapolation. The free energy surfaces are explored for the ESIPT of OHBA in an acetonitrile solution. The free energy profile, especially for the $\pi\pi^*$ state, differs from the gas-phase potential energy curve. In solution, the $\pi\pi^*$ state is below the $n\pi^*$ state for almost entire range of the ESIPT reaction coordinate. The present work indicates that polar solvent controls the relative stability of $\pi\pi^*$ and $n\pi^*$ states.

The RISM-TDDFT method is shown to be a promising approach to examine the photochemical processes in solution. Although actual dynamics does not necessarily follow the minimum free energy path, the proposed method can provide valuable insight into the location of stationary points and the identification of reaction paths. Such static information is a useful guide to the prediction of photochemical processes in solution.

[1]For example, A. DeFusco, N. Minezawa, L. V. Slipchenko, F. Zahariev, and M. S. Gordon, J. Phys. Chem. Lett. **2**, 2184 (2011).
[2]S. Ten-no, F. Hirata, and S. Kato, J. Chem. Phys. **100**, 7443 (1994).
[3]H. Sato, F. Hirata, and S. Kato, J. Chem. Phys. **105**, 1546 (1996).
[4]H. Sato, in *Molecular Theory of Solvation*, edited by F. Hirata (Kluwer Academic, Dordrecht, 2003), pp. 61–99.
[5]K. Naka, A. Morita, and S. Kato, J. Chem. Phys. **110**, 3484 (1999).
[6]S. Yamazaki and S. Kato, J. Chem. Phys. **123**, 114510 (2005).
[7]T. Mori and S. Kato, Chem. Phys. Lett. **437**, 159 (2007).
[8]T. Mori, K. Nakano, and S. Kato, J. Chem. Phys. **133**, 064107 (2010).
[9]S. Gusarov, T. Ziegler, and A. Kovalenko, J. Phys. Chem. A **110**, 6083 (2006).
[10]D. Casanova, S. Gusarov, A. Kovalenko, and T. Ziegler, J. Chem. Theory Comput. **3**, 458 (2007).
[11]D. Yokogawa, H. Sato, and S. Sakaki, J. Chem. Phys. **126**, 244504 (2007).
[12]E. Runge and E. K. U. Gross, Phys. Rev. Lett. **52**, 997 (1984).
[13]M. E. Casida, in *Recent Advances in Density-Functional Methods*, edited by D. P. Chong (World Scientific, Singapore, 1995), p. 155.
[14]K. Burke, J. Werschnik, and E. K. U. Gross, J. Chem. Phys. **123**, 062206 (2005).
[15]M. E. Casida, J. Mol. Struct.: THEOCHEM **914**, 3 (2009).
[16]M. E. Casida and M. Huix-Rotllant, Annu. Rev. Phys. Chem. **63**, 287 (2012).
[17]R. E. Stratmann, G. E. Scuseria, and M. J. Frisch, J. Chem. Phys. **109**, 8218 (1998).
[18]S. Hirata and M. Head-Gordon, Chem. Phys. Lett. **314**, 291 (1999).
[19]F. Furche, J. Chem. Phys. **114**, 5982 (2001).
[20]F. Furche and R. Ahlrichs, J. Chem. Phys. **117**, 7433 (2002).
[21]B. Mennucci, C. Cappelli, C. A. Guido, R. Cammi, and J. Tomasi, J. Phys. Chem. A **113**, 3009 (2009).
[22]D. Jacquemin, B. Mennucci, and C. Adamo, Phys. Chem. Chem. Phys. **13**, 16987 (2011).
[23]M. Cossi and V. Barone, J. Chem. Phys. **115**, 4708 (2001).
[24]R. Cammi, S. Corni, B. Mennucci, and J. Tomasi, J. Chem. Phys. **122**, 104513 (2005).
[25]M. Caricato, B. Mennucci, J. Tomasi, F. Ingrosso, R. Cammi, S. Corni, and G. Scalmani, J. Chem. Phys. **124**, 124520 (2006).
[26]R. Improta, V. Barone, G. Scalmani, and M. J. Frisch, J. Chem. Phys. **125**, 054103 (2006).
[27]Y. Wang and H. Li, J. Chem. Phys. **133**, 034108 (2010).
[28]D. Si and H. Li, J. Chem. Phys. **133**, 144112 (2010).
[29]S. Yoo, F. Zahariev, S. Sok, and M. S. Gordon, J. Chem. Phys. **129**, 144112 (2008).
[30]N. Minezawa, N. De Silva, F. Zahariev, and M. S. Gordon, J. Chem. Phys. **134**, 054111 (2011).
[31]H. Li, J. Chem. Phys. **131**, 184103 (2009).
[32]J. W. Kaminski, S. Gusarov, T. A. Wesolowski, and A. Kovalenko, J. Phys. Chem. A **114**, 6082 (2010).
[33]M. J. F. Fernandez and H. Sato, Theor. Chem. Acc. **130**, 299 (2011).
[34]W. Kohn and L. J. Sham, Phys. Rev. **140**, A1133 (1965).
[35]K. Sneskov, T. Schwabe, O. Christiansen, and J. Kongsted, Phys. Chem. Chem. Phys. **13**, 18551 (2011).
[36]M. W. Schmidt, K. K. Baldridge, J. A. Boatz, S. T. Elbert, M. S. Gordon, J. H. Jensen, S. Koseki, N. Matsunaga, K. A. Nguyen, S. J. Su, T. L. Windus, M. Dupuis, and J. A. Montgomery, Jr., J. Comput. Chem. **14**, 1347 (1993).
[37]M. S. Gordon and M. W. Schmidt, in *Theory and Applications of Computational Chemistry: The First Forty Years*, edited by C. E. Dykstra, G. Frenking, K. S. Kim, and G. E. Scuseria (Elsevier, Amsterdam, 2005), Chap. 41, pp. 1167–1189.
[38]A. D. Becke, J. Chem. Phys. **98**, 5648 (1993).
[39]C. Lee, W. Yang, and R. G. Parr, Phys. Rev. B **37**, 785 (1988).
[40]T. H. Dunning, Jr., J. Chem. Phys. **90**, 1007 (1989).
[41]W. D. Cornell, P. Cieplak, C. I. Bayly, I. R. Gould, K. M. Merz, Jr., D. M. Ferguson, D. C. Spellmeyer, T. Fox, J. W. Caldwell, and P. A. Kollman, J. Am. Chem. Soc. **117**, 5179 (1995).
[42]H. J. C. Berendsen, J. P. M. Postma, M. F. van Gunsteren, and J. Hermans, in *Intermolecular Forces*, edited by B. Pullman (Reidel, Dordrecht, 1981), p. 331.
[43]W. L. Jorgensen and J. M. Briggs, Mol. Phys. **63**, 547 (1988).
[44]D. W. Liao, A. M. Mebel, M. Hayashi, Y. J. Shiu, Y. T. Chen, and S. H. Lin, J. Chem. Phys. **111**, 205 (1999).
[45]U. F. Röhrig, I. Frank, J. Hutter, A. Laio, J. VandeVondele, and U. Rothlisberger, ChemPhysChem **4**, 1177 (2003).
[46]N. S. Bayliss and E. G. McRae, J. Phys. Chem. **58**, 1006 (1954).
[47]A. Balasubramanian and C. N. R. Rao, Spectrochim. Acta **18**, 1337 (1962).
[48]W. P. Hayes and C. J. Timmons, Spectrochim. Acta **21**, 529 (1965).
[49]N. S. Bayliss and G. Wills-Johnson, Spectrochim. Acta A **24**, 551 (1968).
[50]R. F. Borkman and D. R. Kearns, J. Chem. Phys. **44**, 945 (1966).
[51]G. D. Renkes and F. S. Wettack, J. Am. Chem. Soc. **91**, 7514 (1969).
[52]M. O'Sullivan and A. C. Testa, J. Am. Chem. Soc. **92**, 5842 (1970).
[53]L. M. Tolbert and K. M. Solntsev, Acc. Chem. Res. **35**, 19 (2002).
[54]N. Agmon, J. Phys. Chem. A **109**, 13 (2005).
[55]A. Douhal, F. Lahmani, and A. H. Zewail, Chem. Phys. **207**, 477 (1996).
[56]C. J. Seliskar, J. Mol. Spectrosc. **53**, 140 (1974).
[57]J. Catalán, F. Toribio, and A. U. Acuña, J. Phys. Chem. **86**, 303 (1982).
[58]S. Nagaoka, N. Hirota, M. Sumitani, and K. Yoshihara, J. Am. Chem. Soc. **105**, 4220 (1983).
[59]S. Nagaoka, N. Hirota, M. Sumitani, K. Yoshihara, E. Lipczynska-Kochany, and H. Iwamura, J. Am. Chem. Soc. **106**, 6913 (1984).
[60]S. Nagaoka, U. Nagashima, N. Ohta, M. Fujita, and T. Takemura, J. Phys. Chem. **92**, 166 (1988).
[61]S. Nagaoka and U. Nagashima, Chem. Phys. **136**, 153 (1989).
[62]S. Nagaoka, A. Nakamura, and U. Nagashima, J. Photochem. Photobiol., A **154**, 23 (2002).
[63]M. A. Morgan, E. Orton, and G. C. Pimentel, J. Phys. Chem. **94**, 7927 (1990).
[64]M. Čuma, S. Scheiner, and T. Kar, J. Am. Chem. Soc. **120**, 10497 (1998).
[65]S. Lochbrunner, T. Schultz, M. Schmitt, J. P. Shaffer, M. Z. Zgierski, and A. Stolow, J. Chem. Phys. **114**, 2519 (2001).

[66]K. Stock, T. Bizjak, and S. Lochbrunner, Chem. Phys. Lett. **354**, 409 (2002).
[67]A. L. Sobolewski and W. Domcke, Chem. Phys. **184**, 115 (1994).
[68]A. L. Sobolewski and W. Domcke, Phys. Chem. Chem. Phys. **1**, 3065 (1999).
[69]N. L. Doltsinis, Mol. Phys. **102**, 499 (2004).
[70]A. J. A. Aquino, H. Lischka, and C. Hättig, J. Phys. Chem. A **109**, 3201 (2005).
[71]J. D. Coe and T. J. Martinez, Mol. Phys. **106**, 537 (2008).
[72]A. Migani, L. Blancafort, M. A. Robb, and A. D. DeBellis, J. Am. Chem. Soc. **130**, 6932 (2008).
[73]S. P. De, S. Ash, D. K. Bhui, H. Bar, P. Sarkar, G. P. Sahoo, and A. Misra, Spectrochim. Acta, Part A **71**, 1728 (2009).
[74]For example, E.-A. Gould, A. V. Popov, L. M. Tolbert, I. Presiado, Y. Erez, D. Huppert, and K. M. Solntsev, Phys. Chem. Chem. Phys. **14**, 8964 (2012).